Self-limited growth of nanocrystals in phosphosilicate melts during cooling

Liu, S.J.; Lan, S. L.; Tao, H.Z.; Yue, Yuanzheng

Published in:
Journal of the European Ceramic Society

DOI (link to publication from Publisher):
10.1016/j.jeurceramsoc.2019.04.050

Publication date:
2019

Document Version
Accepted author manuscript, peer reviewed version

Title: Self-limited growth of nanocrystals in phosphosilicate melts during cooling

Authors: Shujiang Liu, Shuanglong Lan, Haizheng Tao, Yuanzheng Yue

PII: S0955-2219(19)30288-2
DOI: https://doi.org/10.1016/j.jeurceramsoc.2019.04.050
Reference: JECS 12481

To appear in: *Journal of the European Ceramic Society*

Received date: 26 February 2019
Revised date: 21 April 2019
Accepted date: 26 April 2019

Please cite this article as: Liu S, Lan S, Tao H, Yue Y, Self-limited growth of nanocrystals in phosphosilicate melts during cooling, *Journal of the European Ceramic Society* (2019), https://doi.org/10.1016/j.jeurceramsoc.2019.04.050

Self-limited growth of nanocrystals in phosphosilicate melts during cooling

Shujiang Liu,[a]* Shuanglong Lan[a], Haizheng Tao[b] and Yuanzheng Yue [a,b,c]*

[a]School of Materials Science and Engineering, Qilu University of Technology (Shandong Academy of Science), Jinan 250353, China

[b]State Key Laboratory of Silicate Materials for Architectures, Wuhan University of Technology, Wuhan 430070, China

[c]Department of Chemistry and Bioscience, Aalborg University, DK-9220 Aalborg, Denmark

due to the low network connectivity

Abstract: In this Letter, we demonstrate that the spontaneous nanophase-separation can greatly enhance the heterogeneous nucleation in the investigated phosphosilicate melts. The two separated phases are found to be the phosphate-rich phase as the floppy domain and the silicate-rich phases as rigid phase. We found that sodium phosphate nanocrystals form in the phosphate-rich phase during melt cooling. The growth of these nanocrystals are self-limited, i.e., limited by the surrounding silicate-rich phase with higher viscosity, and hence lower ionic diffusion compared to the phosphate rich phase. Our results show that the substitution of B_2O_3 or Al_2O_3 for partial Na_2O enhances the spontaneous nucleation, although the viscosity of silicate-rich matrix phase is increased by such substitution. This implies that the compositional substitution enhances nanophase separation and thereby lowers the activation energy for non-isothermal crystallization. This work indicates that nanophase separation is crucial for fabrication of transparent glass-ceramics from phosphosilicate melts.

Keywords: Phosphosilicate glass; Melt–cooling–devitrification; Percolation theory; Self-limited crystal growth, Transparent glass ceramics

1. Introduction

The term "glass-ceramics" was first introduced by S.D. Stookey in 1957, with a process-based definition: "…*made by first melting and forming special glasses containing nucleating agents and then causing controlled crystallization of the glass particles*". [1] The traditional glass-ceramic route includes three steps: [2,3] (i) melting, homogenizing, and refining a batch, usually containing one or more nucleating agents; (ii) forming a glass article by hot-shaping (casting, pressing, blowing, rolling, etc.); and (iii) inducing internal crystallization by controlled heat-treatments. Crystallization is a process that involves two separate but interdependent events: nucleation and subsequent crystal growth, and the former is critical for determining crystallization types, e.g., surface or volume crystallizations. In particular, some fluoride-containing silicate glasses exhibit precipitation of fluoride nanocrystals in the floppy regions when the parent glasses were treated at temperatures around glass transition temperature (T_g) [3-5]. The higher viscous domains around crystallites (compared to the matrix phase) ensure that crystals can grow only within nanoscale, since crystal-forming ions cannot migrate to the nucleation sites due to sufficiently high viscosity [5,6]. This viscosity effect has become an effective way to obtain highly transparent glass-ceramics (TGCs) containing nanocrystals, thus offering many potential applications.

Introducing nucleation agents into the compositions or increasing the fraction of the phase-separation can shift the nucleation rate (I) versus temperature curve to higher temperature [7,8], and hence, can enhance spontaneous crystallization during melt-cooling. By varying the melt-cooling rate (q_c), the crystallinity and crystal size distribution in glass can be tuned. However, such a spontaneous crystallization process is hard to be controlled due to rapid nucleation and subsequent crystal growth, and hence, "wild" microstructures can form. This leads to difficulty in tailoring functionalities of glass-ceramics.

Liu et al. demonstrated that highly transparent phosphosilicate glass-ceramics could be prepared via the melt–cooling–devitrification (MCD), i.e., nanocrystals could spontaneously form in the parent melt during controlled cooling [9,10]. The advantages of the MCD approach are manifested by more energy-saving and higher efficiency in production of the transparent glass-ceramics compared to the one- or two-step post heat-treatment on parent glasses. Glass phase-separation plays a key role in inducing heterogeneous nucleation upon cooling of glass melts. [11] Ensuring the size of crystals to be smaller than 100 nm is the prerequisite for achieving high transparency of glass-ceramics since the visible light scattering becomes smaller with decreasing the crystal size [12]. Despite considerable progress in studying nanocrystal formation in glass melts, the origin of the suppressed growth of nanocrystals has not been fully clarified, particularly for silicate systems. Such clarification will be critical for precisely tailoring the functionalities of glass materials for targeted applications.

In the present work, we prepare the highly transparent phosphosilicate glass-ceramics containing nanocrystals via MCD approach using relatively low cooling rate, i.e., the cooling rate of cast-forming process. The glass-ceramics have following nominal composition (mol%): 62 SiO_2 - 4 P_2O_5 - (20-x) Na_2O - 7 MgO - 7 ZnO - x (B_2O_3 or Al_2O_3) with x=0 or 4. We provide experimental evidence for preferential formation of the nanocrystals in the separated phosphate-rich glassy phase as floppy region. To reach this goal, we investigate the effect of substitution of B_2O_3 or Al_2O_3 for partial Na_2O on the spontaneous crystallization behavior. This study will be beneficial to optimizing the conditions for fabricating transparent glass-ceramics containing nanocrystals.

2. Experimental

The batches of reagent grade chemicals (SiO_2, $(NH_4)_2HPO_4$, Na_2CO_3, MgO, ZnO, H_3BO_3 and Al_2O_3) were

preheated at 673 K for 12 hours and at 1273 K for 2 hours to remove NH_3 and CO_2, and then completely melted in a lidded platinum crucible placed in an electric furnace at 1773–1823 K for 2 h. Subsequently, the melts were cast onto stainless steel molds to obtain bulk samples with the thickness of 6.0 mm, and afterwards naturally cooled down to room temperature in air. In addition, fast-quenched samples were also obtained by pouring the glass melts into cold water, and their amorphous nature was verified by XRD analysis. In order to realize full crystallization, the as-cast bulk samples were also heat-treated at T_g for different time of periods. The chemical compositions of the samples were determined using X-ray fluorescence (XRF) as listed in Table 1.

The effect of B_2O_3 or Al_2O_3 addition on transparency of the as-cast bulk samples was characterized in terms of light transmittance in the visible range. The transmittance was measured using a UV–VIS-NIR Specord 200 spectrophotometer (Analytik Jena AG, Jean) at a resolution of 1 nm. The thickness of samples for transmittance measurements is 1.00 ± 0.05 mm.

To study the non-isothermal melt-crystallization behavior, differential scanning calorimetry (DSC) (STA 449F, Net-zsch) was used to measure the enthalpy evolution of five samples of each glass during downscans. Each of the samples was individually upscanned in the DSC from 333 to 1573 K at 20 K min^{-1} and kept at 1573 K for 20 min, then cooled to room temperature at 10, 15, 20, 25 to 30 K min^{-1}, respectively. Thus, the characteristic temperatures, e.g., peak temperature (T_{peak}) and onset temperatures (T_{onset}) of crystallization event as well as liquidus temperature (T_L) were determined from the DSC curves. To determine glass transition temperature (T_g), all the fast-quenched samples underwent two runs of up- and downscans at 10 K/min, and T_g values were determined from the second upscan DSC curve (see Table 1) [13,14].

In order to identify the crystalline phases of as-cast and heat-treated bulk samples, x-ray powder diffraction

(XRD) measurements were performed on the central part of the samples using an x-ray diffractometer (BRUKER AXS D8-Advance) with graphite monochromatized Cu $K_{\alpha 1}$ radiation. High-resolution transmission electron microscopy (HRTEM) observations were performed using a JEOL 2100F microscope equipped with a field emission gun (200 KeV) and a high-resolution UHR pole piece. The samples for TEM imaging were prepared by cutting the samples to slices, then grinding the slices to the thickness of 30–50 μm, and finally thinning them by bombardment of Ar^+ ion-beam. For SEM (FEI Quanta 200) observations, fractured cross-section of bulk samples was etched in 5 wt% HNO_3 solution for 10 seconds.

Equilibrium viscosities in the high-temperature range were measured using the SRV-1600 cylinder concentric viscometer (Orton SRV-1600) under the atmospheric air. During cooling, the melt viscosity values were determined at an interval of 50 K. The melt was kept for 30 min at each temperature to reach a stable uniform temperature, and hence, to obtain the accurate viscosity values.

3. Results and discussion

3.1 Formation of nanocrystals upon cooling

The high visible light transparency of the three as-cast bulk samples was realized via the melt–cooling–devitrification (MCD) method. As shown in Fig. 1, the three bulk samples exhibit the light transmittance of about 90% in the wavelength range of visible light. The high transparency of the Al_2O_3 containing glass sample is demonstrated in the inset of Fig. 1. However, two sharp diffraction peaks appear at 2θ = 22 and 34° in the XRD patterns of the three bulk samples (Fig. 2a), indicating occurrence of crystalline phases during the casting processes. The main crystalline phase is identified to be Na_3PO_4 (PDF: 31-1323) for the three samples. Specially, the partial substitution of B_2O_3 or Al_2O_3 for Na_2O leads to a prominent increase in intensity of the diffraction peaks, i.e., to increased crystallization tendency. Considering the same cooling histories for the

three samples, the glass composition difference must be responsible for the enhanced tendency to spontaneous crystallization. Furthermore, XRD patterns of the samples heat-treated at their respective T_gs for 40 h are shown in Fig. 2(b). It is seen that the crystal type in the heat-treated samples is same with that in the as-cast samples. However, the pronounced bumps of the XRD patterns indicates the presence of a large amount of amorphous phase for all the samples.

High-resolution TEM (HRTEM) micrographs of three as-cast bulk samples are presented in Fig. 3, in which highly dispersive particles can be observed. The Na_2O-containing sample contains dots with the size of ca. 6-10 nm (Fig. 3a), and clear crystallographic planes, i.e., the long-range order arrangements of ions, can be observed in the magnified image, indicating the crystalline nature of the dots. However, the partial substitution of B_2O_3 or Al_2O_3 for Na_2O results in a drastic increase in quantity of crystallites accompanied by a slight decrease in mean nanocrystal size, i.e., 3-7 nm for both the B_2O_3 and the Al_2O_3 containing samples (Figs 3b and c). In addition, the size of nanocrystals is found to vary in a narrow range for each sample, even though the mean particle sizes of the three samples are different. This suggests that nucleation is so fast during cooling that many nanocrystals form simultaneously, leading to the approximately identical size for the majority of nanocrystals. Undoubtedly, such small nanocrystals ensures weak scattering of visible light, and hence, high transparency of the samples [15].

3.2 Non-isothermal crystallization dynamics upon cooling

To explore the origin of the enhancement of crystallization tendency by partial B_2O_3 or Al_2O_3 substitution for Na_2O in the glass system, DSC downscans were conducted on the three samples at different cooling rates (q_c) from above liquidus (T_L) to room temperature. Fig. 4 shows the downscan curves of three melts at 10, 15, 20, 25 to 30 K min^{-1}, respectively. A strong exothermal peak due to crystallization event is seen in the Na_2O

containing glass for all the cooling rates, and it shifts to lower temperature with increasing the melt cooling rate, as indicated by the change of the peak temperature (T_{peak}) (Table 2). However, the partial substitution of B_2O_3 or Al_2O_3 for Na_2O leads to an apparent shift of T_{peak} to lower and higher temperature, respectively. In addition, the onset (T_{onset}) temperatures at various cooling rates are determined as the temperatures corresponding to the crystallinities of 1% (Table 2). Thus, the apparent incubation period (Δt_{inc}) of crystallization is defined as the period during which the sample is in the molten state, viz. $\Delta t_{inc} = (T_L - T_{onset})/q_c$. As exhibited in Table 2, Δt_{inc} is found to monotonically increase with decreasing the cooling rate for all the three samples. This is because a higher cooling rate gives a higher undercooling degree (ΔT), and hence, the change of the Gibbs free energy from melt to crystal becomes more negative, meaning a larger thermodynamic driving force for nucleation.

Furthermore, to judge the ability of the glass melts to crystallize during cooling, the apparent activation energy for crystallization was determined using the Kissinger equation [16]:

$$\ln\left(\frac{\alpha}{T_{peak}^2}\right) = -\frac{E}{RT_{peak}} + C \qquad (1)$$

where α and T_{peak} are the cooling rate of DSC downscans and the temperature of exothermic peak, respectively, E is the apparent activation energy for crystallization, R is the gas constant, and C is a constant. According to Eq. (1), $\ln(\alpha/T^2_{peak})$ is linearly plotted against $1/T_{peak}$ (Fig. 5), and then the E value can be calculated from the slope (Table 2). It is seen that the partial substitution of B_2O_3 or Al_2O_3 for Na_2O leads to a decrease of E, especially for the substitution of B_2O_3 for Na_2O. Since E is a measure of the energy barrier for crystallization, the lower E values for the B_2O_3 or Al_2O_3 containing glasses implies that the melt-crystallization can be drastically enhanced by the partial substitution of B_2O_3 or Al_2O_3 for Na_2O.

3.3 Self-limited growth mechanism

In a melt-crystallization process, a large extent of overlapping between the growth rate (u) versus T curve and the nucleation rate (I) versus T curve favors spontaneous crystallization [17]. Previous studies demonstrated that phosphosilicate glasses had complex short-range order structure, and tended to separate into phosphate- and silicate-rich glass phases owing to the competition in attracting oxygen ions between the two network former ions (P^{5+} and Si^{4+}) [18,19]. Phase-separation in turn enhances heterogeneous nucleation, thereby increasing the overlapping extent of u(T) and I(T) curves. In this work, SEM measurements were also performed on the cross-sections of the as-cast samples etched by H_3NO_3 to identify the phase-separation. As shown in Fig. 6, in contrast to the Na_2O containing sample, in which no obvious signature of phase-separation can be found, the matrixes of both the B_2O_3 containing and the Al_2O_3 containing samples possess evenly distributed spherical pits with size of 60-80 nm. Formation of these pits could be explained by the fact that HNO_3 tends to preferentially attack the separated phosphate-rich phase. This means that introduction of B_2O_3 or Al_2O_3 into the glass enhances phase-separation tendency. However, discrete Na_3PO_4 crystals cannot be observed in the SEM micrographs of three samples, though there are strong XRD peaks for the three bulk samples (Fig. 2a). This might be due to the possible scenario that the crystals are mainly incorporated into the phosphate-rich phase, and the latter is easily removed by HNO_3.

According to the percolation theory, where the glass structure can be considered to be an arbitrarily formed network with rigid and floppy regions [20,21], the heat-treatment around T_g could cause glasses to preferentially crystallize in the floppy regions associated with lower network connectivity since floppy regions have lower viscosity than rigid ones. NMR studies showed that P^{5+} always exists in an orthophosphate complex in phosphosilicate melts independent of the P_2O_5 content [22,23]. The unique coordination of P^{5+} results in the low connectivity of network in phosphate-rich phase, i.e., floppy region. To confirm the fact that Na_3PO_4

crystals preferentially form in the phosphate-rich phase upon cooling the glass melts, isothermal heat-treatments were performed on the as-cast bulk samples at their respective T_gs for different durations (t), i.e., 5, 10, 20, 30 to 40 h. Note that all the heat-treated samples were still highly transparent independent of t. Subsequently, DSC measurements were conducted on the samples both before and after heat-treatment for 40 h. From the solid DSC upscan curves (20 K min^{-1}) in Figs. 7a-c, we see a weak crystallization peak (denoted by the arrow) for each as-cast bulk sample. The change of the crystallization degree with t can be described by that of crystallization enthalpy (ΔH) as a function of t [6]. ΔH of each heat-treated sample can be determined by calculating the crystallization peak area. ΔH data are plotted as a function of t in Fig. 7(d). It is seen that ΔH value decreases monotonically with extending t, and reaches to nearly zero at t=20 h for the three samples, indicating cease of the crystallization process, i.e., termination of crystal growth. This is confirmed by absence of the crystallization peaks on the DSC curves of the samples heat-treated for 40 h (dashed lines in Figs. 7a-c). Considering the above SEM results, the dependence of crystallization degree on t demonstrates that heat-treatment at T_g can causes crystals to further grow in phosphate-rich phase, but at the same time the high viscosity of the silicate-rich matrix phase around the nanocrystals limits the overgrowth of nanocrystals. In addition, the similarity of XRD patterns between the as-cast and the heat-treated samples for 40 h (see Figs. 2a and 2b) also implies that the formation of Na_3PO_4 crystals in the phosphate-rich phase easily occurs during cooling of the glass melts, and their growth is limited by the rigid silicate-rich phase.

To further verify our inference and explanation, we compare the equilibrium viscosity (η) data among the three studied glass compositions in a wide temperature range. In the high-temperature region, the temperature dependences of η for the three glass composition are illustrated in Fig. 8, where an increase in η is seen when B_2O_3 or Al_2O_3 is introduced, and in particular, Al_2O_3 causes an even larger increase in η. Note that the

equilibrium viscosity could not be directly measured in the low-temperature range due to the invention of strong melt crystallization, and thus, only the viscosity point at T_g, i.e., 10^{12} Pa s [13,14] is shown. Subsequently, the $\log_{10}\eta$ versus T curve in a wide temperature range is obtained by fitting the viscosity data to the Mauro-Yue-Ellison-Gupta-Allan (MYEGA) equation [22]. From the fitting curves of three glass melts (dashed lines in Fig. 8), the viscosities of the B_2O_3 or Al_2O_3 containing phosphosilicate melts are higher than those of the only Na_2O containing melt in the entire temperature region (800 to 1800 K). It is known that viscosity plays an important role since it is linked to the kinetic barrier for both nucleation and crystal growth. However, the overall composition-viscosity relation cannot explain why the crystallization is enhanced by partial substitution B_2O_3 or Al_2O_3 for Na_2O, since it is unlikely that high viscosity favors nucleation and crystal growth. Therefore, the phase separation should be the main reason for the enhanced crystallization, particularly for nucleation process. In other words, crystallization takes place in the phosphate-rich phase rather than silicate-rich phase, the increase in η which is mainly associated with the latter has little effect on spontaneous crystallization.

4. Conclusions

We investigated the crystallization behavior of undercooled phosphosilicate melts by partially substituting B_2O_3 or Al_2O_3 for Na_2O. The separated phosphate-rich phase was considered to be floppy region because of lower network connectivity compared to the silicate-rich phase, and the latter phases retarded the growth of crystalline phases, thus ensuring the formation of sufficiently small crystals, and hence high transparency of the glass-ceramics. In addition, partial substitution of B_2O_3 or Al_2O_3 for Na_2O favors the spontaneous formation of sodium phosphate nanocrystals due to the enhanced phase-separation, even though the viscosity of matrix silicate-rich phase is increased. This work provides insight into the formation mechanism of transparent glass-ceramics, and benefits both the tailoring of the functionalities of transparent glass-ceramics, and the

optimization of the fabrication conditions.

Acknowledgements

This work was financially supported by Shandong Provincial Major Scientific and Technological Innovation Project, China (2018YFJH0402), and National Natural Science Foundation of China (Nos: 51772223, 51372180).

References

[1] S.D. Stookey, History of the development of pyroceram, Res. Manag. 1 (1958) 155–163.

[2] X.F. Liu, J.J. Zhou, S.F. Zhou, Y. Y.Yue, J.R. Qiu, Transparent glass-ceramics functionalized by dispersed crystals, Prog. Mater. Sci. 97 **(**2018) 38-96.

[3] C.G. Lin, C. Bocker, C. Rüssel, Nanocrystallization in oxyfluoride glasses controlled by amorphous phase separation, Nano Lett. 15 (2015) 6764–6769.

[4] S. Bhattacharyya, C. Bocker, T. Heil, J.R. Jinschek, Th. Hoche, C. Rüssel, H. Kohl, Experimental evidence of self-limited growth of nanocrystals in glass, Nano Lett. 9 (2009) 2493-2496.

[5] I. Avramov, R. Keding, C. Rüssel, Crystallization kinetics and rigidity percolation in glass-forming melts, J. Non-Cryst. Solids 272 (2000) 147–153.

[6] S. J. Liu, Y. Kong, H. Z. Tao, Y. H. Sang, Crystallization of a highly viscous multicomponent silicate glass: rigidity percolation and evidence of structural heterogeneity, J. Euro. Ceram. Soc., 37 (2017) 715–720.

[7] S. Krüger, J. Deubener, Stochastic nature of the liquid-to-crystal heterogeneous nucleation of supercooled lithium disilicate liquid. J Non-Cryst Solids 388 (2014) 6-9.

[8] S. Krüger, J. Deubener, The TTT curves of the heterogeneous and homogeneous crystallization of lithium disilicate–Astochastic approach to crystal nucleation. Front Mater. 3 (2016) 42.

[9] S.J. Liu, G.Z. Fu, Z.T. Shan, X.R. Ren, Y.F. Zhang, C.F. Zhu, W. He and Y.Z. Yue, Nanocrystal formation and photoluminescence in the Yb^{3+}/Er^{3+} codoped phosphosilicate glasses, J. Non-Cryst. Solids 383 (2014) 141-145.

[10] S.J. Liu, Z.T. Shan, G.Z. Fu and Y.Z. Yue, Influence of rare earth oxides on the non-isothermal crystallization of phosphosilicate melts during cooling, J. Non-Cryst. Solids 385 (2014) 75-80.

[11] W. Holand, G. Beall. Glass-ceramic Technology. American Ceramic Society. Westerville, OH, 2002.

[12] G.H. Beall, D.A. Duke, Transparent glass-ceramics, J. Mater. Sci., 4 (1969) 340-352.

[13] Y.Z. Yue, Characteristic temperatures of enthalpy relaxation in glass, J. Non-Cryst. Solids 354 (2008) 1112-1118.

[14] Y.Z. Yue, The iso-structural viscosity, configurational entropy and fragility of oxide liquids, J. Non-Cryst. Solids 355 (2009) 737–744

[15] H.P. Klug, L.E. Alexander, X-ray Diffraction Procedures: For Polycrystalline and Amorphous Materials, Wiley, New York, 1974.

[16] H. E. Kissinger, Reaction kinetics in differential thermal analysis, Anal. Chem. 1957; 29: 1702-1706

[17] S.J. Liu, H.Z. Tao, Y.F. Zhang, Y.Z. Yue, A new approach for determining the critical cooling rates of nucleation in glass-forming liquids, J. Am. Ceram. Soc. 100 (2017) 3875–3882.

[18] J.M. Oliveira, R.N. Correia, M.H. Fernandes, Effect of SiO_2 on amorphous phase separation of CaO–P_2O_5–SiO_2–MgO glasses, J. Non-Cryst. Solids 273 (2000) 59-63.

[19] T. Hoche, C. Moisescu, I. Avramov, C. Rüssel, W.D. Heerdegen, Microstructure of $SiO_2-Al_2O_3-CaO-P_2O_5-K_2O-F^-$ Glass Ceramics. 1. Needlelike versus Isometric Morphology of Apatite Crystals, Chem. Mater. 13 (2001) 1312-1219.

[20] M.F. Thorpe, continuous deformations in random networks, J. Non-Cryst. Solids 57 (1983) 355-370.

[21] J.C. Philipps, M.F. Thorpe, Constraint theory, vector percolation and glass formation, *Solid State Commun*., 53 (1985) 699-702.

[22] H. Grussaute, L. Montagne, G. Palavit, J.L. Bernard, Phosphate speciation in $Na_2O–CaO–P_2O_5–SiO_2$ and $Na_2O–TiO_2–P_2O_5–SiO_2$ glasses, J. Non-Cryst. Solids 263 (2000) 312-317.

[23] M. D. O'Donnell, S.J. Watts , R.V. Law, R.G. Hill, Effect of P_2O_5 content in two series of soda lime phosphosilicate glasses on structure and properties – Part I: NMR, J. Non-Cryst. Solids, 354 (2008) 3554-3560.

[24] J.C. Mauro, Y.Z. Yue, A.J. Ellison, P.K. Gupta and D.C. Allan, Viscosity of glass-forming liquids, PNAS 106 (2009) 19780–19784.

Figure 1. Light transmittance curves of the as-cast bulk samples obtained by melt–cooling–devitrification (MCD) approach. Comparisons were made among the Na_2O containing sample, the $Na_2O+B_2O_3$ containing one and the $Na_2O+Al_2O_3$ containing one.

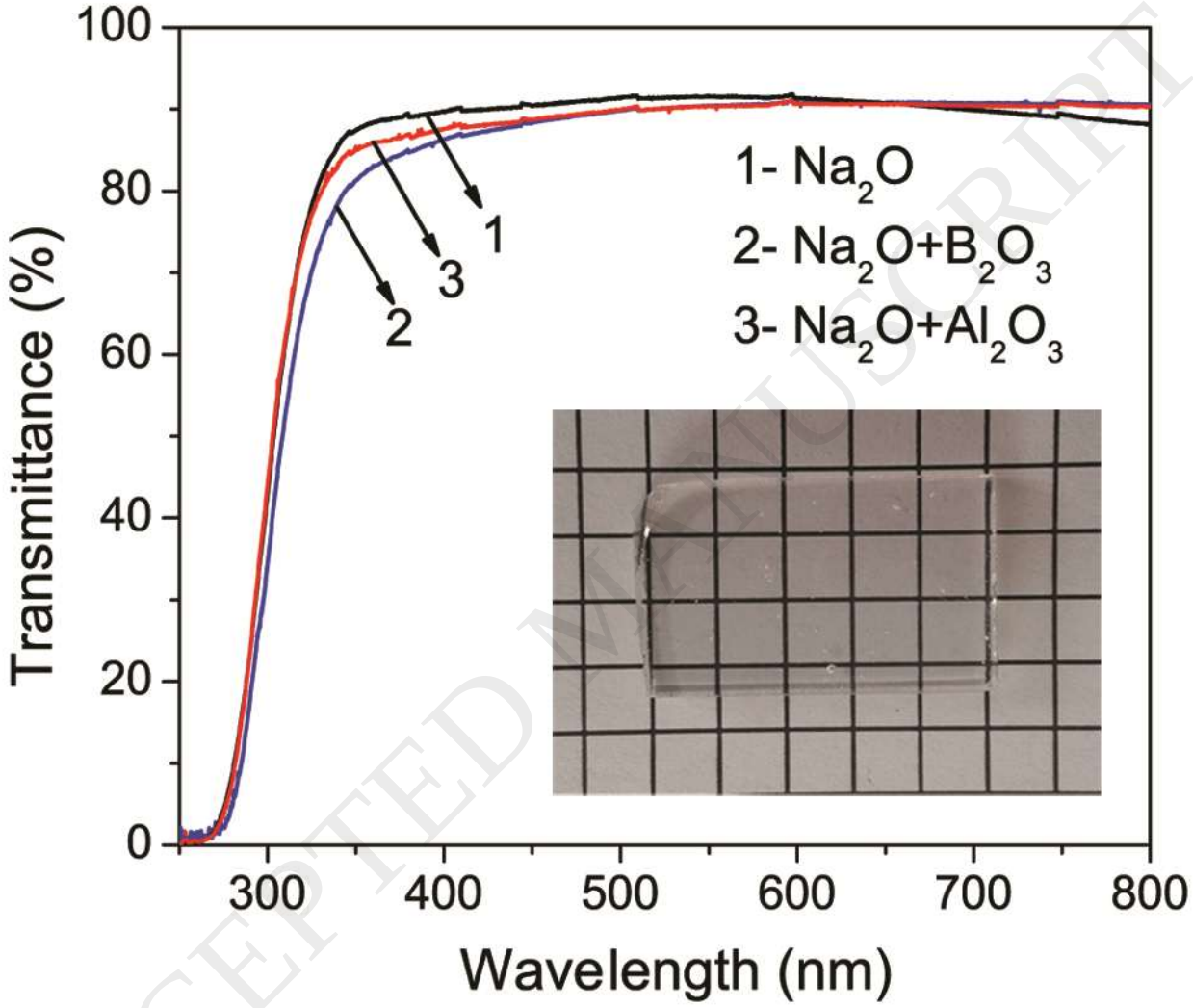

Figure 2. XRD patterns of the as-cast bulk glass-ceramics samples (a) and those heat-treated for 40 h (b) for three compositions such as Na_2O containing, the $Na_2O+B_2O_3$ containing and the $Na_2O+Al_2O_3$ containing one.

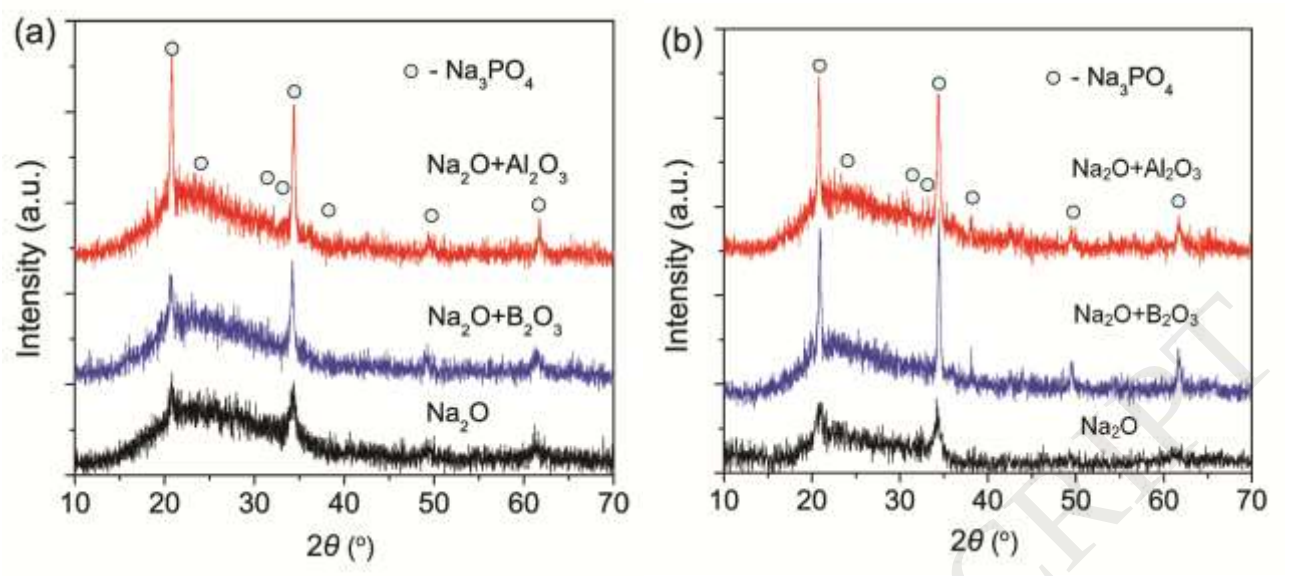

Figure 3. TEM images of the transparent bulk samples with three compositions: containing Na_2O (a), containing $Na_2O+B_2O_3$ (b) and containing $Na_2O+Al_2O_3$ (c). The scale bar is 10 nm for all the images. Inset of Fig. 3a: the magnified image of dots.

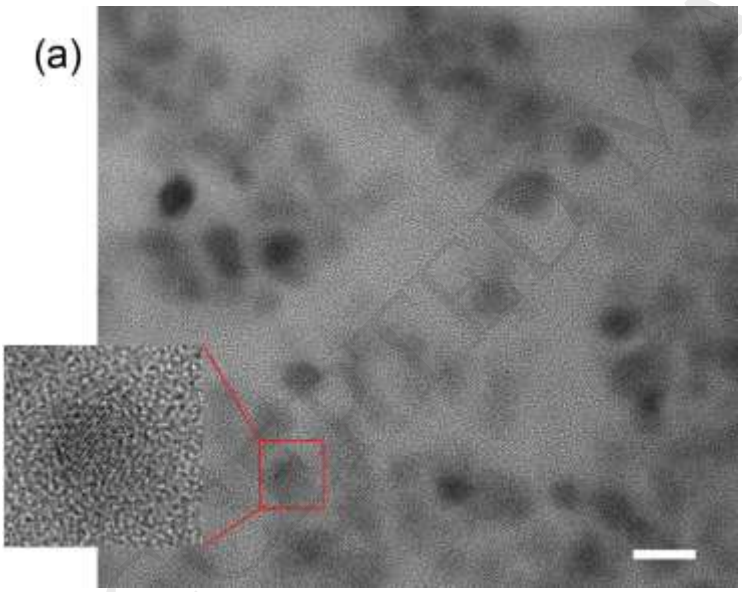

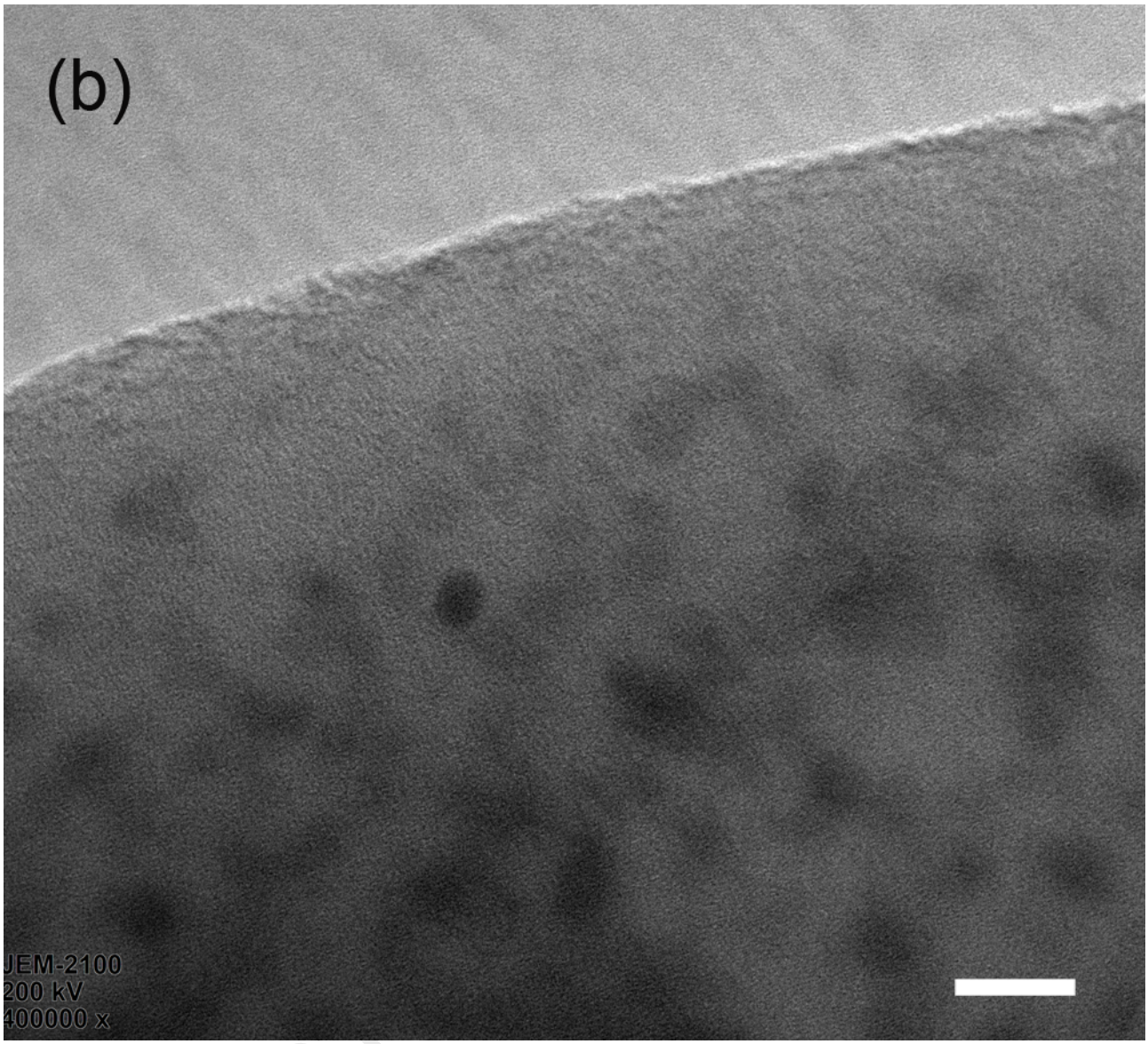

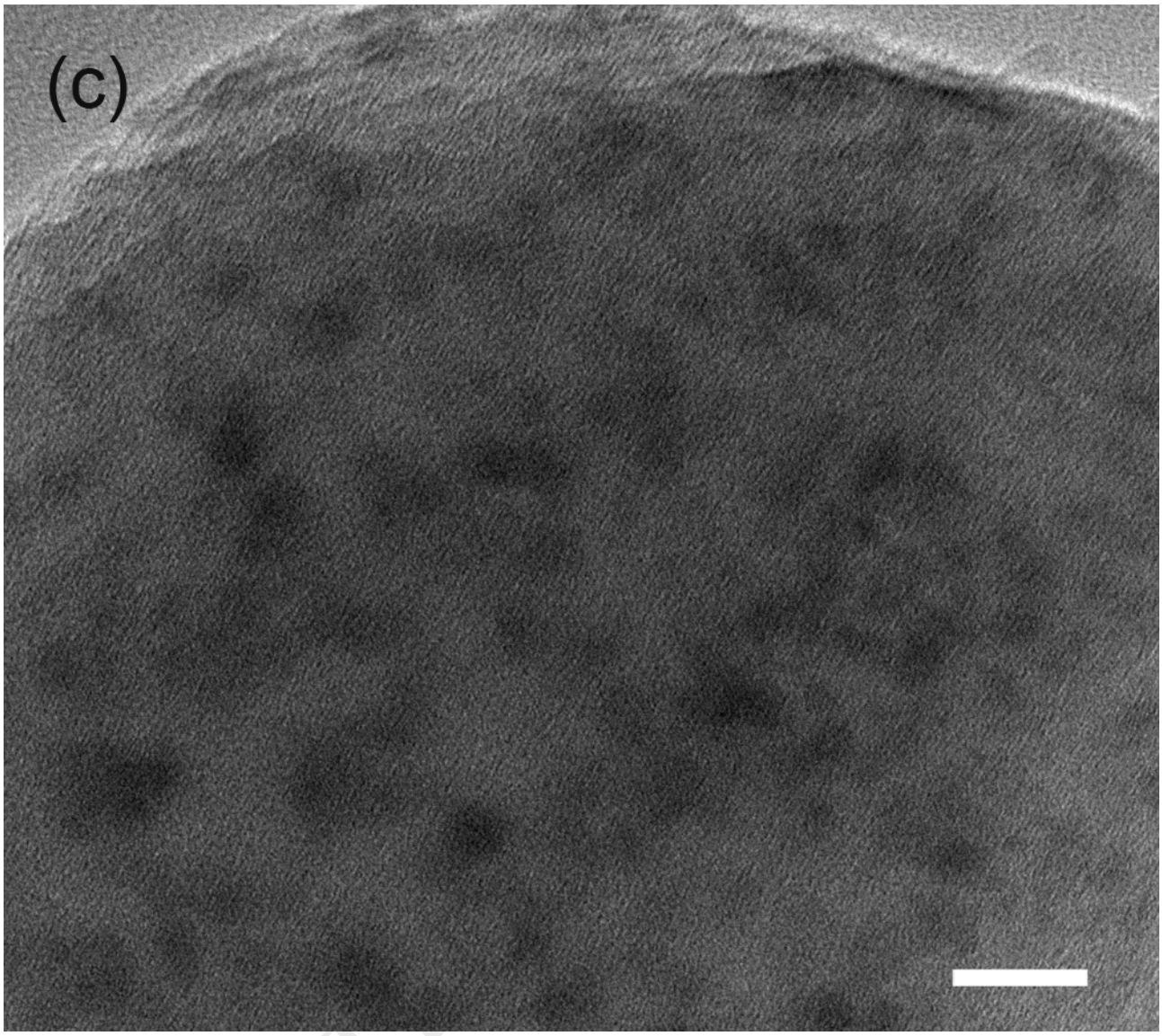

Figure 4. Downscan heat flow curves obtained at different cooling rates for the glass melts containing Na_2O (a), $Na_2O+B_2O_3$ (b) and $Na_2O+Al_2O_3$ (c).

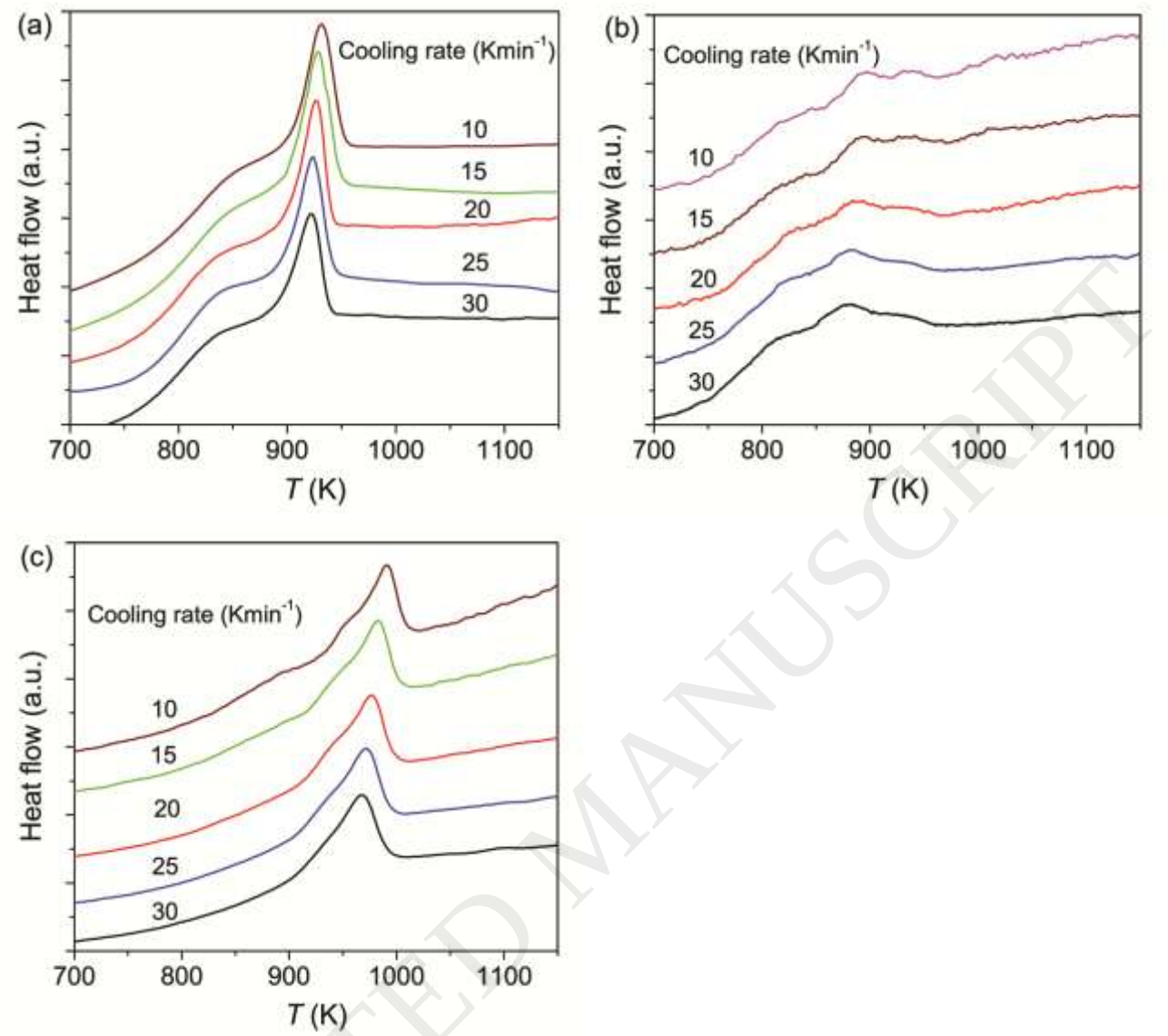

Figure 5. The plots of ln (α/T_{peak}^2) versus 1000/T_{peak} for the melt containing Na_2O (squares), containing Na_2O+B_2O_3 (circles) and containing Na_2O+Al_2O_3 (triangle). Solid lines: linear fits.

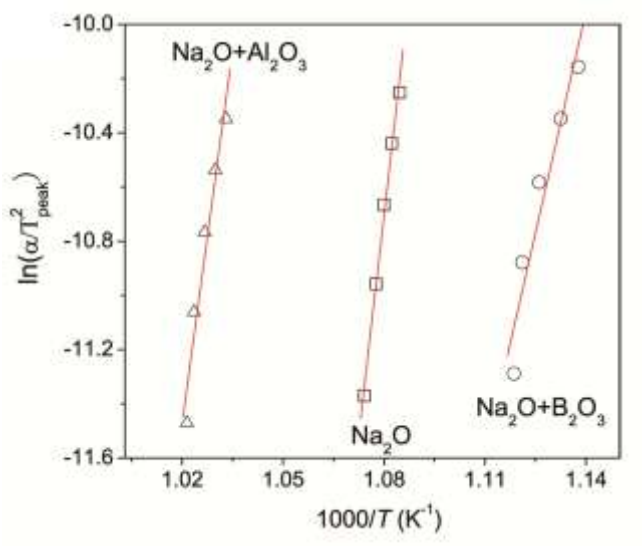

Figure 6. SEM images of the three transparent samples containing Na_2O (a), B_2O_3 (b) and Al_2O_3 (c), respectively.

The cross-sections of samples were etched by 5% HNO_3 for 15 s. The scale bar is 200 nm for all the images.

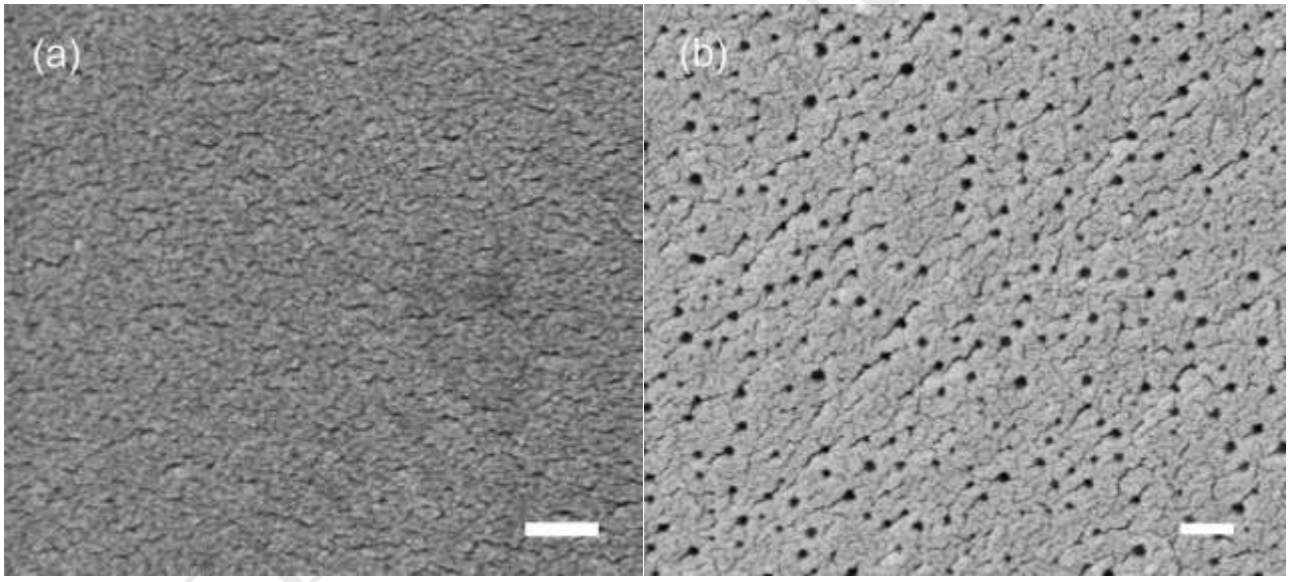

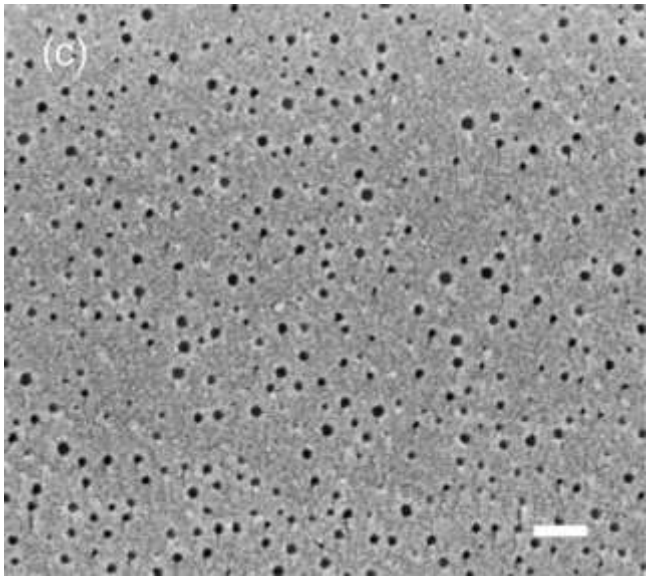

Figure 7. Heat flow curves obtained during DSC upscans at 20 K min^{-1} for the three studied bulk samples before and after heat-treatment for 40 h. (a) Na_2O containing sample; (b) B_2O_3 containing sample; (c) Al_2O_3 containing sample. (d) Dependences of the enthalpy for crystallization on the heat-treatment duration (t) at their respective T_gs.

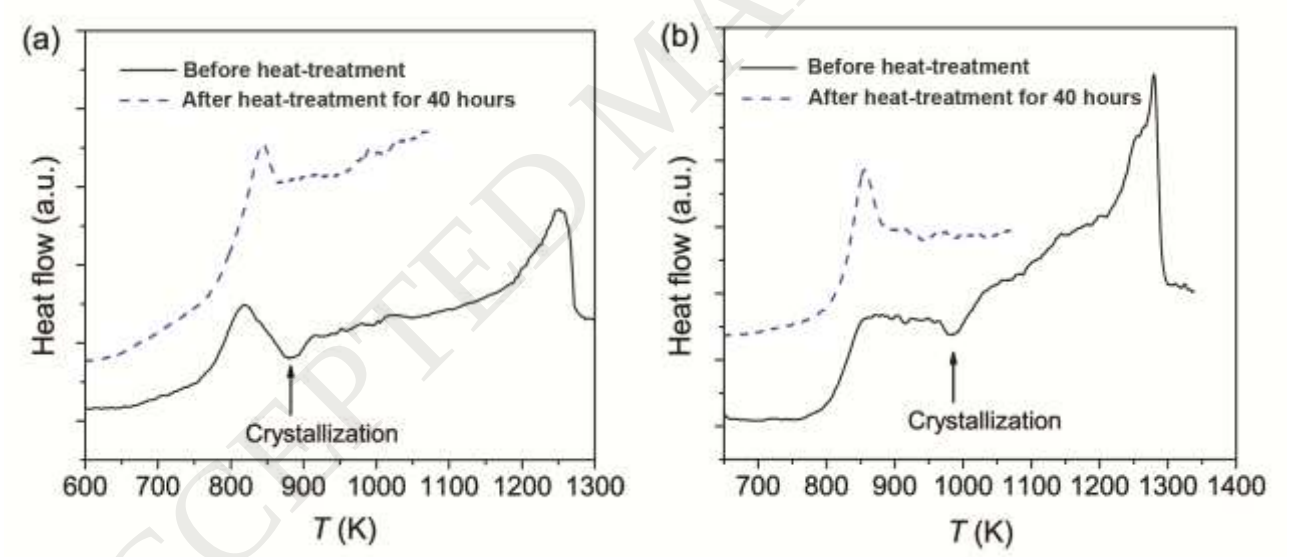

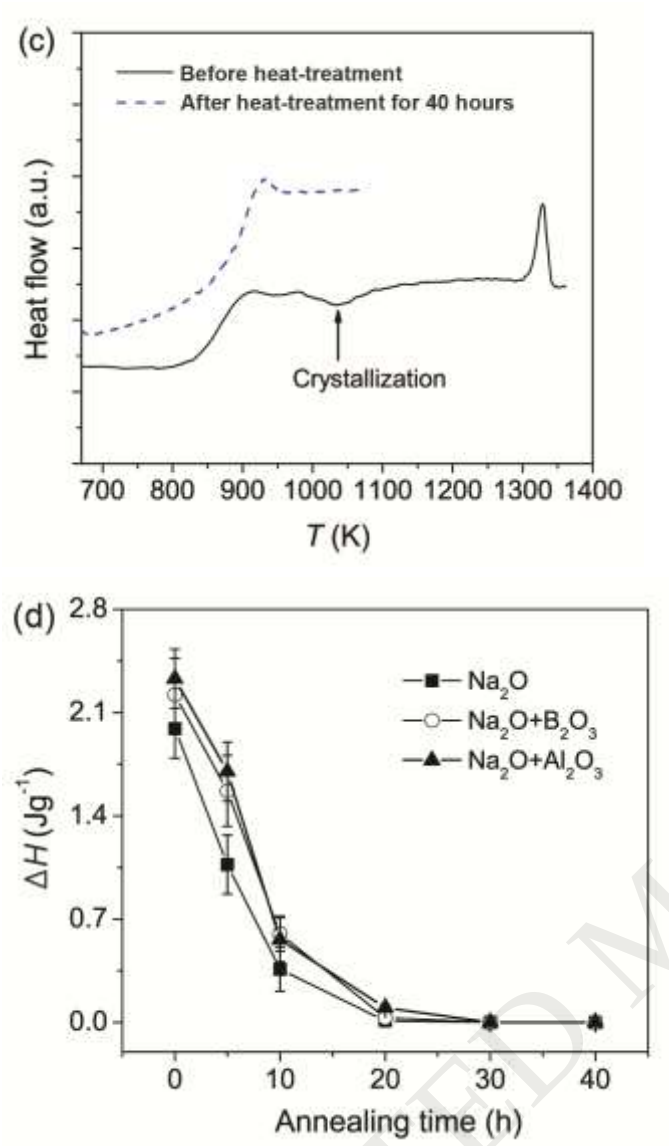

Figure 8. The temperature dependences of viscosity for the three studied glass compositions. Dashed lines: the fit of the MYEGA equation to the viscosity data. The T_g values (corresponding to the viscosity of 10^{12} Pa s) were determined from the second DSC curve of the fast-quenched samples.

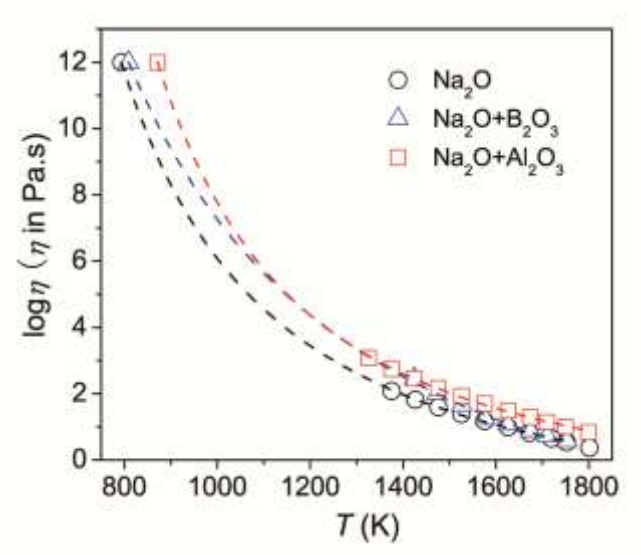

Table 1. Analyzed chemical compositions (mol%), and glass transition temperature (T_g) determined by DSC.

Sample No.	SiO_2	P_2O_5	Na_2O	MgO	ZnO	B_2O_3	Al_2O_3	T_g (K)
Na_2O	62.51	3.89	19.76	5.82	8.02	-	-	793
Na_2O+ B_2O_3	63.00	3.99	15.67	5.76	7.73	3.85	-	809
Na_2O+ Al_2O_3	62.08	3.86	16.09	5.76	8.08	-	4.13	871

Table 2. Characteristic values for the non-isothermal melt-crystallization for the three studied compositions and apparent activation energy for crystallization.

α (K min^{-1})	Na_2O			
	Δt_{inc} (min)	T_{onset} (K)	T_{peak} (K)	E (kJ mol^{-1})
30	11.04±0.02	938±2	922±1	
25	13.31±0.03	940±2	924±1	
20	16.71±0.02	941±2	926±1	898±44
15	21.87±0.03	943±2	928±1	
10	32.67±0.02	944±2	931±1	

α (K min^{-1})	Na_2O + B_2O_3			
	Δt_{inc} (min)	T_{onset} (K)	T_{peak} (K)	E (kJ mol^{-1})
30	10.89±0.02	951±2	879±1	
25	13.15±0.02	952±2	883±1	
20	16.02±0.03	953±2	888±1	451±75
15	22.31±0.02	955±2	892±1	
10	34.01±0.03	957±2	894±1	

α (K min^{-1})	Na_2O + Al_2O_3			
	Δt_{inc} (min)	T_{onset} (K)	T_{peak} (K)	E (kJ mol^{-1})
30	13.36±0.02	994±2	968±1	
25	15.46±0.03	995±2	971±1	
20	20.88±0.03	996±2	974±1	765±89
15	30.42±0.02	998±2	977±1	
10	48.43±0.03	1000±2	979±1	